Solid Earth
Discussions
Open Access
EGU

1 **Structural features derived from a Multiscale Analysis and 2.75D Modelling of**

2 **Aeromagnetic Data over the Pitoa-Figuil Area (Northern Cameroon)**

3

4

5 Voltaire Souga Kassia[a]; Theophile Ndougsa Mbarga[a,b*];Arsène Meying[c]; Jean Daniel Ngoh[a]; Steve

6 Ngoa Embeng [a]

7

8 [a]Postgraduate School of Science, Technology and Geosciences, University of Yaoundé I, Yaoundé, Cameroon

9 [b]Department of Physics, Advanced Teacher's Training College, University of Yaoundé I, P.O. Box 47, Yaoundé, Cameroon

10 [c]School of Geology and Mining Engineering, University of Ngaoundéré, P.O. Box 115, Meiganga, Cameroon

11

12 Correspondence should be addressed to Ndougsa Mbarga Theophile; *tndougsa@yahoo.fr

13

14

15 **ABSTRACT:**

16 In the Pitoa-Figuil area (Northern Cameroon), an interpretation of aeromagnetic data was

17 conducted. The aim of this investigation was first to emphasize lineaments hidden under geological

18 formations and secondly to propose two 2.75D models of the subsurface structures. Different

19 magnetic data processing techniques were used, notably horizontal gradient magnitude, analytic

20 signal, and Euler deconvolution. These techniques in combination with the 2.75D modelling to the

21 aeromagnetic anomaly reduced to the equator permit to understand the stratification of the deep

22 and near surface structures, which are sources of the observed anomalies. We managed to put in

23 evidence and characterize 18 faults and some intrusive bodies. According to Euler's solutions,

24 anomaly sources go up to a depth of 5.3 km.

25 **Keywords:** Horizontal gradient magnitude, Euler deconvolution, 2.75D modelling, Fault, Intrusive

26 body.

27

28

29 **1. Introduction**

30 Investigating depths through geomagnetic field properties is the basis of the magnetic

31 method, the one we used for this research.

32 This study is focused on a well-defined area in the northern Cameroon. Several studies

33 (Ntsama et al., 2014; Kamguia et al., 2005) reveal the presence of many Cretaceous sedimentary

34 basins. At the beginning of the Cretaceous age, the basement of the northern Cameroon region was

35 affected by a tectonic event due to the Benue trough set up, which generated faults that promote

36 volcanic activities (Ntsama et al., 2014). The resulting basaltic lava flows and the accumulated

37 alluvial deposits in Mayos buried these faults.

38 The aim of this research paper is firstly to highlight magnetic anomalies and correlate them

39 with the tectonic and geological events given by existing literature in order to locate and identify

40 buried faults. Secondly, this article tries to make its contribution to the knowledge of the

41 stratification of the Pitoa-Figuil subsurface. To achieve these purposes, some techniques such as
42 Analytic signal, Euler deconvolution and 2.75D modelling were applied.
43
44 **2. Geological and tectonic setting**
45   Fragment of the Pan-African Belt in the northern part of Cameroon, between the longitudes
46 13°30' - 14°15' E and latitudes 09°15' - 09°45' N, the studied area covers several cities among which
47 the most historical are Pitoa and Figuil. The basement complex consists of migmatite and ectinitic
48 rocks from the Precambrian. The sedimentary basins in and around the studied area were set up in
49 the Cretaceous by the NE-SW Benue trough which is one of the direct consequences of the
50 establishment of the gigantic moat covered by the Atlantic Ocean (Ntsama et al., 2014).
51   The various geological formations and structures of the said zone are identified on Fig. 1 and
52 can be grouped as follows (Toteu et al., 2004):
53   - Superficial formations (Q^3) from the Quaternary age;
54   - Cretaceous sedimentary formations (Ci, Cm);
55   - Precambrian formations namely ectinites (ξ^1, ξ^2, ζ^1, ζ^2), migmatites (M^1, M^2), ancient
56   eruptive rocks (γ^1, γ^2) and micaceous quartzites.
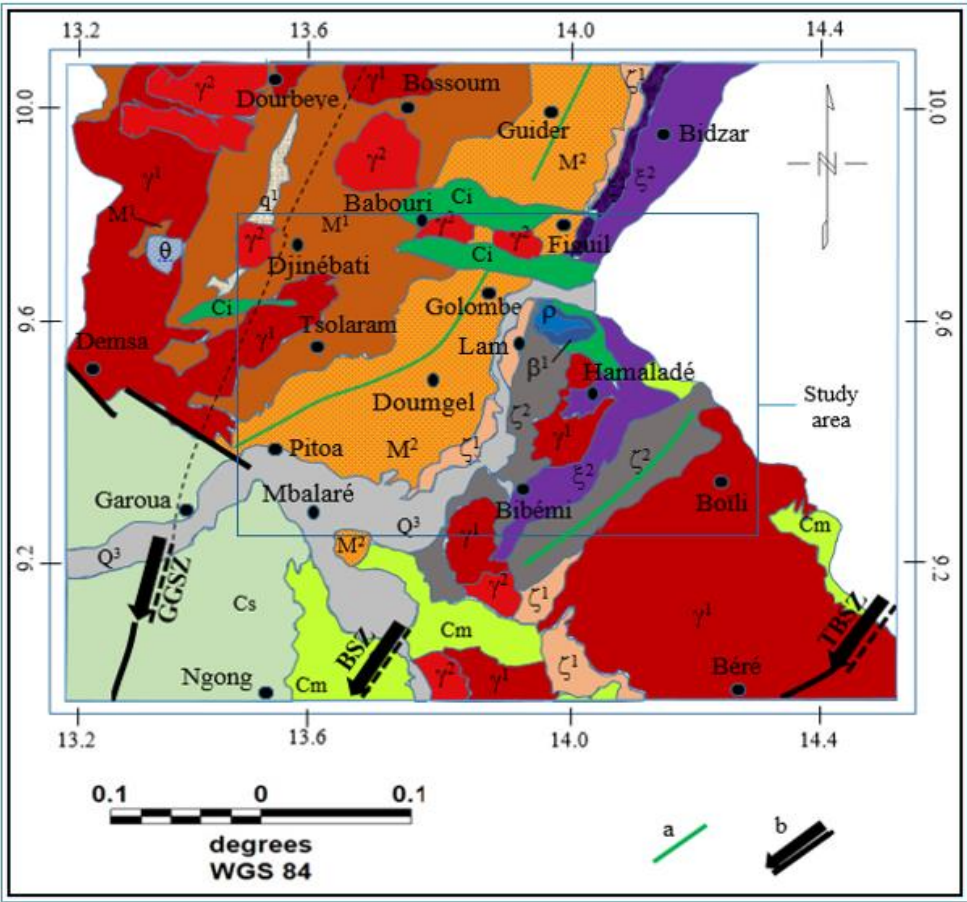57   Effusive rocks are also present, notably the rhyolites and rhyolitic tuffs of the Tertiary, as well
58 as the undifferentiated monchiquite basalts of the Benue valley which are from the Cretaceous age.
59   The Mayo Oulo-Léré basin (Ci), which is the eastward branch of the Benue trough, extends for
60 about 50 km (length) with a width value for about 9 km (Ntsama et al., 2014).
61   Two NE-SW tectonic lines mark the studied area: one at the west of Boïli and the other at the
62 West of Golombe. Most dips are vertical. The migmatite gneisses formation at the geological map
63 centre is intruded by a NE-SW veins of quartz. Ntsama et al. (2014) revealed the presence of faults
64 buried under geological formations. Most orthogneisses and migmatites come from the
65 transformation of granitoids due to the Panafrican deformation D2 (Daouda, 2014).
66   On the structural aspect, the northern Cameroon domain is marked by two deformation
67 phases (Toteu et al., 2004):
68   - The first phase is characterised by a foliation with variable dip and direction;
69   - The second one is characterised by tight and straight folds associated to a vertical axial
70   plane foliation.

Figure 1: Geological map of the studied area (redrawn from Ngako et al., 2008; Elangwe, 1979 ; this map is available at the public domain): (γ^1) Anatexia granites and granodiorites; (γ^2) Monzonitic late syntectonic granites; (M^1) Biotite anatexite; (M^2) Migmatitic gneisses; (ζ^1) Lower gneisses: biotite, amphibole and pyroxene cross-cut by intrusive quartz; (ζ^2) Upper gneisses: grenatiferous with two micas; (ξ^1) Lower micaschists of the Poli Group; (ξ^2) Upper micaschists with chlorites of the Poli Group; (q^1) Micaceous quartzites; (β^1) Undifferentiated monchiquite basalts of the Bénoué valley; (Q^3) Alluviums and lacustrine clays; (θ) Gabbros; (ρ) Ryolites and ryolitic tuffs; (Ci) Amakassou and Kontcha sandstone conglomerate and schisto-clays; (Cm) Bénoué and Kontcha sandstone; (Cs) Garoua sandstone; (a) Tectonic lines; (b) Shear zones: Godé-Gormaya shear zone (GGSZ), Tcholliré-Banyo shear zone (TBSZ).

3. Materials and methods

In 1970, aeromagnetic data were collected by the company SURVAIR (Canada) for the Federal Republic of Cameroon. After correction of data resulting from this survey, Paterson et al. (1976**)**, established magnetic maps and included them in their final report. These magnetic maps are the starting point and the key component of this study. We used MapInfo v11.0 to digitize them. Then, through the Oasis montaj software v8.4, we subtracted the International Geomagnetic Reference Field (IGRF) from the measured field to obtain the total magnetic intensity (TMI).

3

Solid Earth
Discussions
Open Access
EGU

88   In the present paper, data filtering techniques were implemented using the Oasis montaj
89   software v8.4.
90
3.1. Reduction to Magnetic Equator
92   For further data interpretation, the reduction to magnetic equator (RTE) technique is much
93   more used in the equatorial zones to centre the magnetic anomalies in line with their sources.
94   The RTE is calculated following Eq. (1) (Leu, 1981):

95    $$R(\vartheta) = -\frac{\left[A(I) - i\cos(I).\cos(D-\theta)^2\right] \times \cos^2(D-\theta)}{\left[A^2(Ia) + \varphi^2(Ia,D)\right] \times \left[A^2(I) + \varphi^2(I,D)\right]} \qquad (1)$$

96   Where:
97   I is the geomagnetic inclination;
98   D is the geomagnetic declination;
99    $A(I) = sin(I)$ is the RTE amplitude;
100   $\Phi(I,D) = cos(I).cos(D-\vartheta)$ is the RTE phase;
101   Ia is the inclination for RTE amplitude correction.
102   The RTE technique was applied to the TMI anomalies where -2.588° were used as the
103   inclination value and -4.132° as declination at 1st January 1970 which is the date corresponding to
104   the period of which data were collected.
105
3.2. Horizontal Gradient Magnitude
107   The horizontal gradient magnitude (HGM) is a filtering technique usually used for potential
108   fields. It makes it possible to highlight lithological contacts of bodies in basement.
109   The HGM is given by Eq. (2) (Cordell and Grauch, 1982):

110   $$HGM\,(x,\,y) = \sqrt{\left(\frac{\partial M(x,y)}{\partial x}\right)^2 + \left(\frac{\partial M(x,y)}{\partial y}\right)^2} \qquad (2)$$

111   Where the magnetic field is $M\,(x,\,y)$.
112   Vertical body edges are generally located through the maxima of HGM (Awoyemi et al., 2016).
113
3.3. Analytic Signal Method
115   The strong magnetizations of the analytic signal (AS) make it possible to highlight limit
116   contacts of geological formations. The AS amplitude of magnetic anomaly is defined by Eq. (3)
117   (Roest et al., 1992):

118   $$|AS(x,\,y)| = \sqrt{\left(\frac{\partial M(x,y)}{\partial x}\right)^2 + \left(\frac{\partial M(x,y)}{\partial y}\right)^2 + \left(\frac{\partial M(x,y)}{\partial z}\right)^2} \qquad (3)$$

119   The fact that the AS is a function always positive and therefore, does not require to know the
120   direction of the magnetized body, is a major advantage of this technique compared to the others
121   (Jeng et al., 2003).
122
3.4. Euler Deconvolution
124   Applied to aeromagnetic data, it is a technique which permits to locate sources of observed
125   anomalies and determine their depths. This technique is based on an important parameter that

Solid Earth
Discussions

126 accounts for the degree of homogeneity of the mathematical equation that comes into play, this
127 parameter is named "structural index" (Durrheim, 1998). The structural index (SI) characterizes the
128 geological type of the source (dyke, sill, pipe, cylinder, and sphere) according to its value which
129 varies between 0 and 3 for the case of magnetic data.

130 The Euler's homogeneity equation in this case is the Eq. (4) below (Whitehead and
131 Musselman, 2005):

132

133 $(x\text{-}x_0)\left(\frac{\partial T}{\partial x}\right) + (y\text{-}y_0)\left(\frac{\partial T}{\partial y}\right) + (z\text{-}z_0)\left(\frac{\partial T}{\partial z}\right) = N(M\text{-}T)$ (4)

134 Where:

135 (T) is the total magnetic field produces at *(x, y, z) by* the magnetic source at (x_0, y_0, z_0);

136 M is the regional value of T;

137 N is the structural index (SI).

138 With four unknown parameters (x, y, z, M), solving the Euler's equation requires to consider a
139 square window on the grids of gradients and field. However, this window must be sized to exclude
140 unwanted anomalies while containing all significant solutions (Durrheim, 1998).

141

142 **3.5. 2.75D modelling**

143 When a source of anomalies presents a preferred extension in a given direction, profiles are
144 interpreted perpendicularly to the main extension. The 2.75D model represents geological blocks as
145 polygonal prisms either finite or infinite elongated following a strike direction named Y with
146 horizontal axes (X). The plane of the profile and the Y direction need not to be perpendiculars
147 (Rasmussen and Pedersen, 1979).

148 According to Skalbeck et al. (2005), the 2.75D modelling is a potential field modelling
149 technique based on asymmetric strike length (Y) about the profile (X). The 2.75D modelling
150 techniques are suitable for geological modelling, as potential field profiles may not cross a structure
151 through its centre.

152 To build our magnetic models, we used the analyses of Talwani and Heirtzler (1964) and
153 Rasmussen and Pedersen (1979). These models were obtained through GM-SYS™ which is an
154 extension of Geosoft package software v8.4.

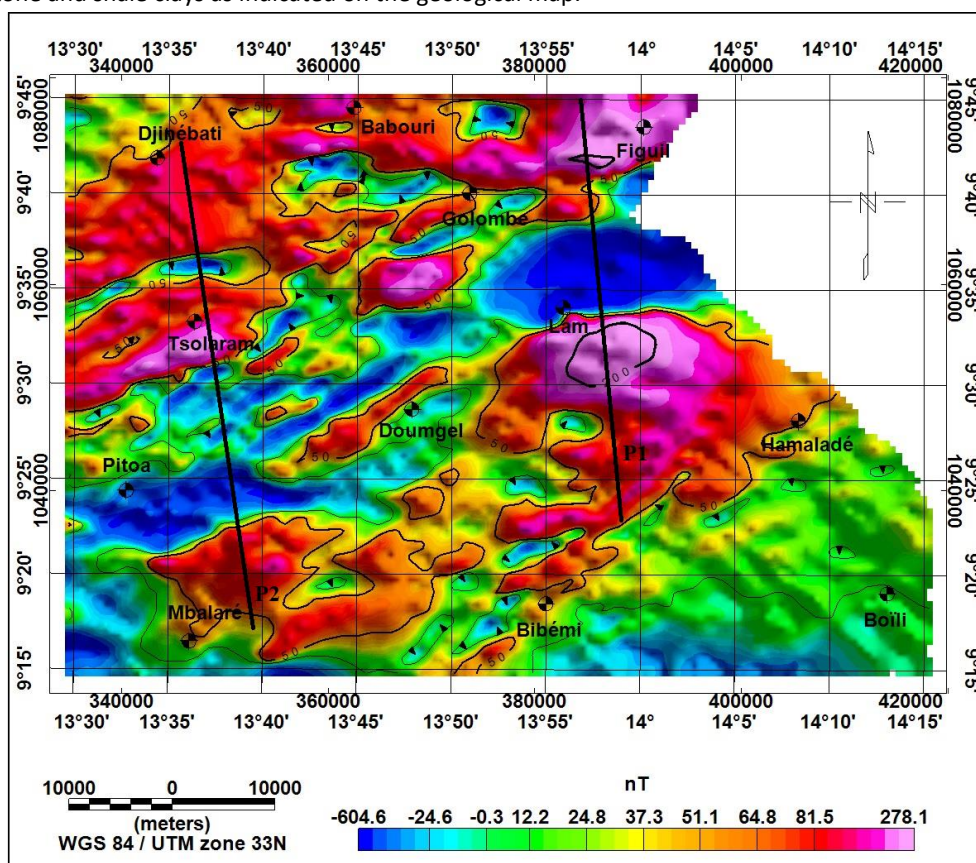155

156 **4. Results**
157 **4.1. RTE map**

158 The map (Fig. 2) presents an irregular distribution of anomalies. The values in nanotesla (nT)
159 of these anomalies range from -660.3 to 286.4 with various forms. It is thus possible to distinguish
160 positive magnetic anomalies (dark pink and red colour) which are in great proportion on this map
161 and a minority of negative magnetic anomalies (light and dark blue colour) which lodge the NE-SW
162 axis.

163 The Lam area is marked by an elliptical bipolar anomaly with an E-W direction over a length of
164 about 15.5 km. This anomaly has an intensity of -600 nT for the negative pole and 200 nT for the
165 positive pole which is more developed than the negative one. The positive pole at this point
166 correlates well with the geological map (Fig. 1), which indicates the presence of monchiquite basalts

167 of the Benue valley and rhyolitic tuffs which are rocks with a strong magnetic response. In short,
168 these are anomalies that materialize the signature of a geological structure buried under the covers.
169 The negative lobe suggests the presence of geological formations with low susceptibilities such as
170 sandstone and shale clays as indicated on the geological map.

171

Figure 2: Color shaded reduction to equator (RTE) map.

173 The same observation is made in south of Pitoa where this time we have -400 nT for the
174 negative pole and about 75 nT for the positive one with a mainly ENE-WSW direction.

175 In the western Doumgel, between the two previous bipolar anomalies, there is a group of
176 small positive (70 nT) and negative (-500 nT) linear anomalies with ENE-WSW direction. The forms
177 and directions of these anomalies and those of the southern Pitoa allow us to believe that they
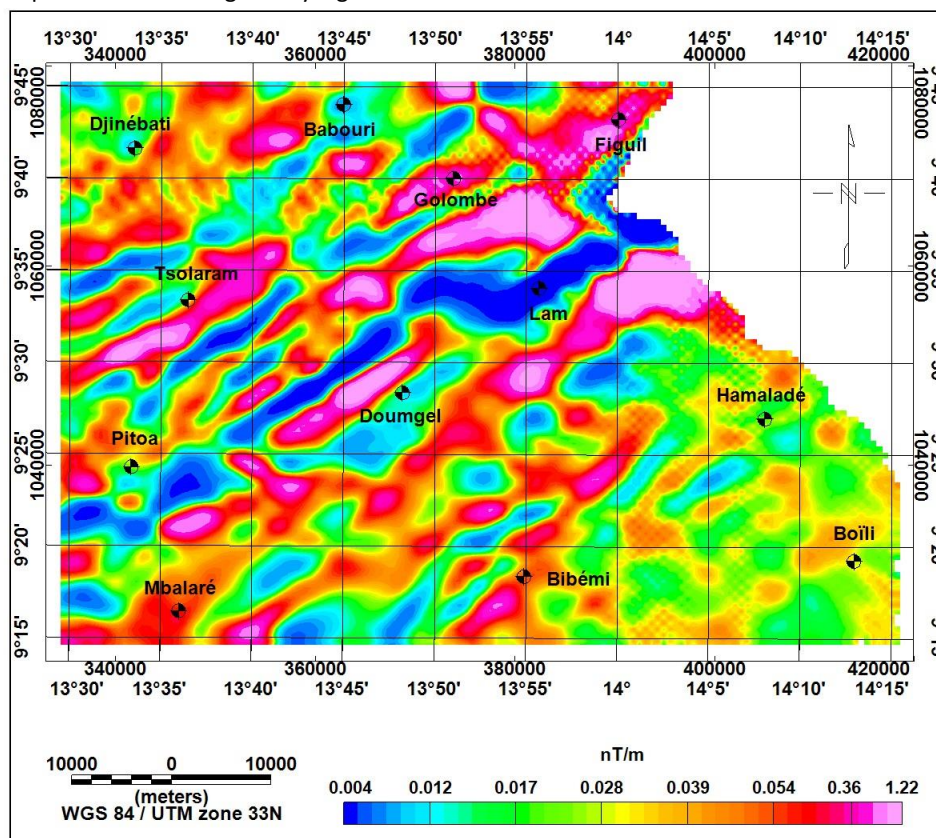178 would be the outcome of the same tectonic event.

179 From the magnetic point of view, the subsurface in Northern Cameroon is perturbed by
180 several anomalies with different wavelengths, most of them are related to the Precambrian
181 basement formations. Some anomalies reflect sedimentary deposits. Bipolar anomalies could be
182 interpreted as very deep geological structures hidden by extensive formations (Feumoe et al.,
183 2012).

Solid Earth
Open Access
Discussions
EGU

184
185 **4.2. HGM map**

186   The horizontal gradient magnitude technique is a great way to locate geological contacts in
187 the basement and faults by determining their directions (Khattach et al., 2006). To better
188 distinguish deeper geological structures, the HGM method is applied to the 2 km upward continued
189 RTE map and the result is given by Fig. 3.

190
191 **Figure 3: Horizontal Gradient Magnitude (HGM) map.**

192   There is a wide variety of anomalies, most of them are linear with different lengths and their
193 amplitudes fluctuate between 0.004 and 1.22 nT/m.

194   The corresponding structures are mainly oriented in the NE-SW direction. Some elliptical and
195 unformed anomalies around Figuil and at the northern Tsolaram are plainly observable. Outcrops or
196 intrusive bodies can explain the high level of the amplitude gradients which characterize them.
197 Many linear and curved bipolar magnetic anomalies are observed along the Pitoa-Figuil axis. Viewed
198 their form, some of these anomalies are certainly magnetic responses of dykes or faults.

199   For automatic location of the HGM maxima, we adopted the Blakely and Simpson (1986)
200 method. The resulting map (Fig. 5) shows that local maxima (green peaks) form narrow wrinkles
201 above abrupt susceptibility fluctuations.

202   On the centre of the map, more precisely in the area covered by the migmatite gneisses, the
203 configuration of the NE-SW maxima suggests the presence of structural deformation at the regional
204 scale in the basement stratums. This correlates well with the linear anomalies of the RTE map and
205 are interpreted as being the direct consequences of the settlement of the Benue tectonic trough
206 due to the opening of the Atlantic.

207

208 **4.3. AS map**
209   The AS method is applied to the 2 km upward continued RTE map and the result is given by
210 Fig. 4. The high magnetic signals of the AS map correlate well with the magnetic response of
211 migmatite rocks found in the Lam area and around the Figuil-Pitoa axis with a NE-SW trend.
212 Geological contacts represented by harsh signal contrasts are emphasized; among them, appears
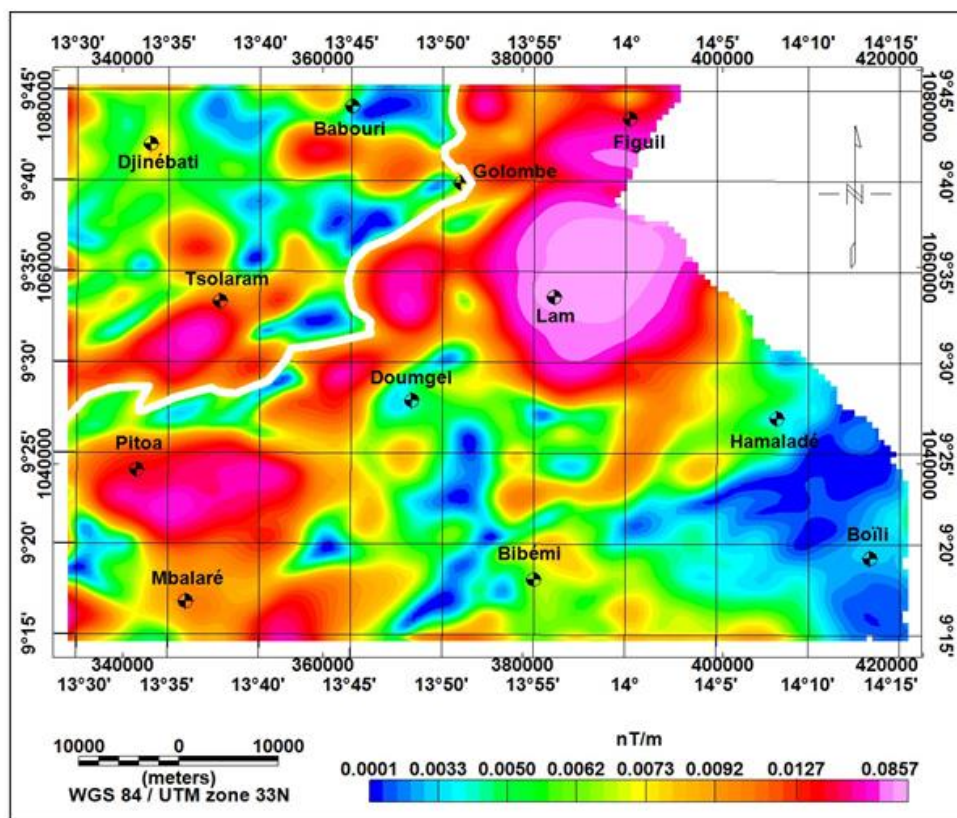213 the biotite anatexite - migmatite gneisses contact (white outline).

214

215   **Figure 4: Analytic signal (AS) map.**

216

217   AS and HGM maxima were generated, pooled, and superimposed in a single map as shown on
218 Fig. 5. Peaks are quasi-parallel, it is the proof that the geological structures of our study region
219 admit dips linked to dextral and senestral deformations which affected it (Ngako et al., 2008). The

220 maxima of the HGM are more abundant than those of the AS. According to Cordell and Grauch
221 (1982), areas where the AS maxima are isolated, indicate the much deeper structures (southern
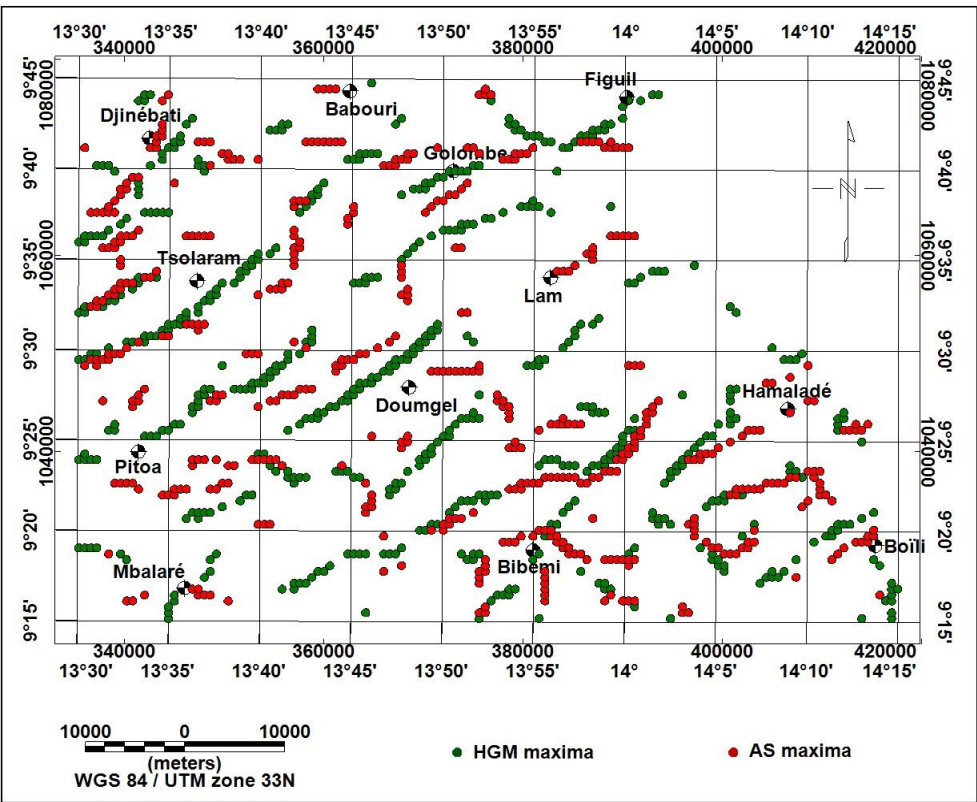222 Pitoa, Doumgel and Lam area).

223

224 **Figure 5: HGM (in green) and AS (in red) peaks map.**

225

4.4. Euler's solutions map

227   The 2 km upward continued RTE map is the map on which was applied the Euler
228 deconvolution method, to determine depths of anomaly sources by setting the flying height of
229 plane observation at 235 m, the tolerance at 15% and the structural index at 1. Given the
230 importance of the wavelength of anomalies and the value of the grid cell, we have chosen a Nyquist
231 window size of 15 km × 15 km. The result is given by Fig. 6 below.

232   On the Euler's solutions map above, several structures with depth varying from 1400 to 5300
233 m are highlighted. We can clearly distinguish deep faults and intrusive bodies which are
234 characterized by the non-linear or the stacking of Euler's solutions (Keating and Pilkington, 2004;
235 Ndougsa et al., 2012). This is observed in the Lam area and southern Pitoa. Some of these intrusive
236 bodies are located around the contact zone between the biotite anatexite and the migmatite
237 gneisses stratums at a depth of about 4000 m. From this same interpretation, intrusive bodies at

238 almost the same depth, are also perceived nearby the contact zone between upper gneisses and
239 upper mica schists formations in the Eastern Bibémi.
240   As for rectilinear and continuous alignments of Euler's solutions found in the northern and
241 western areas, they would be the magnetic signatures of normal faults hidden under geological
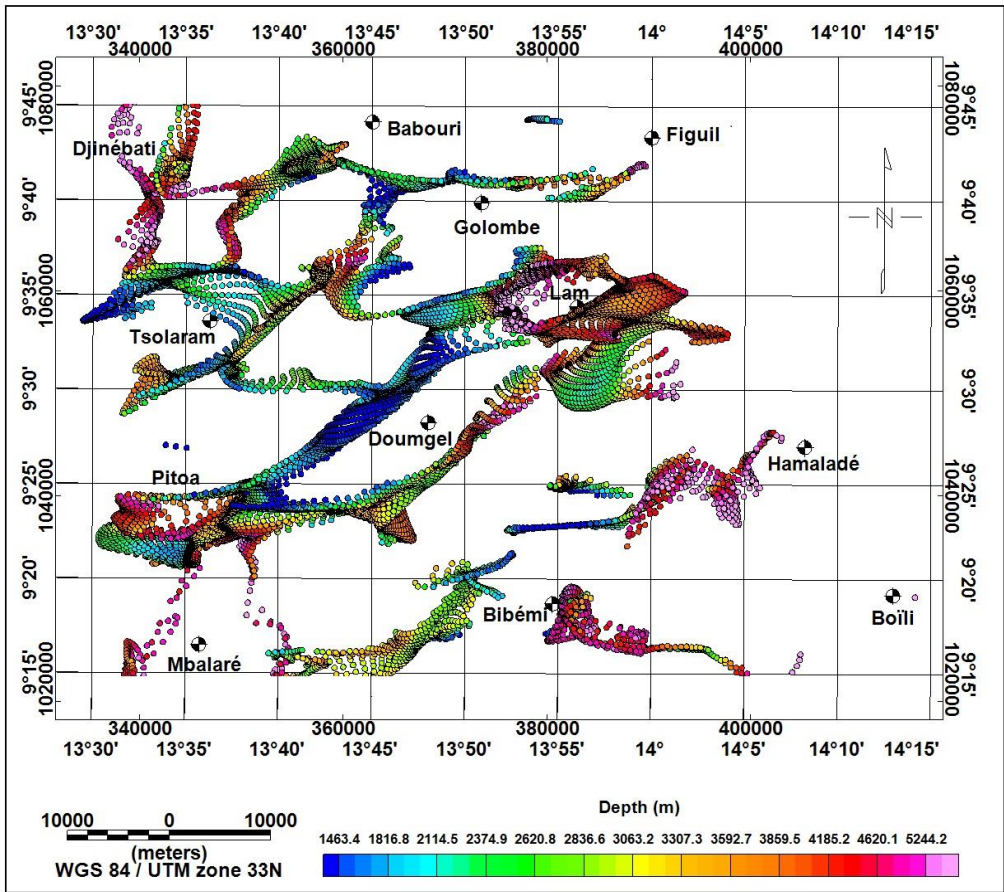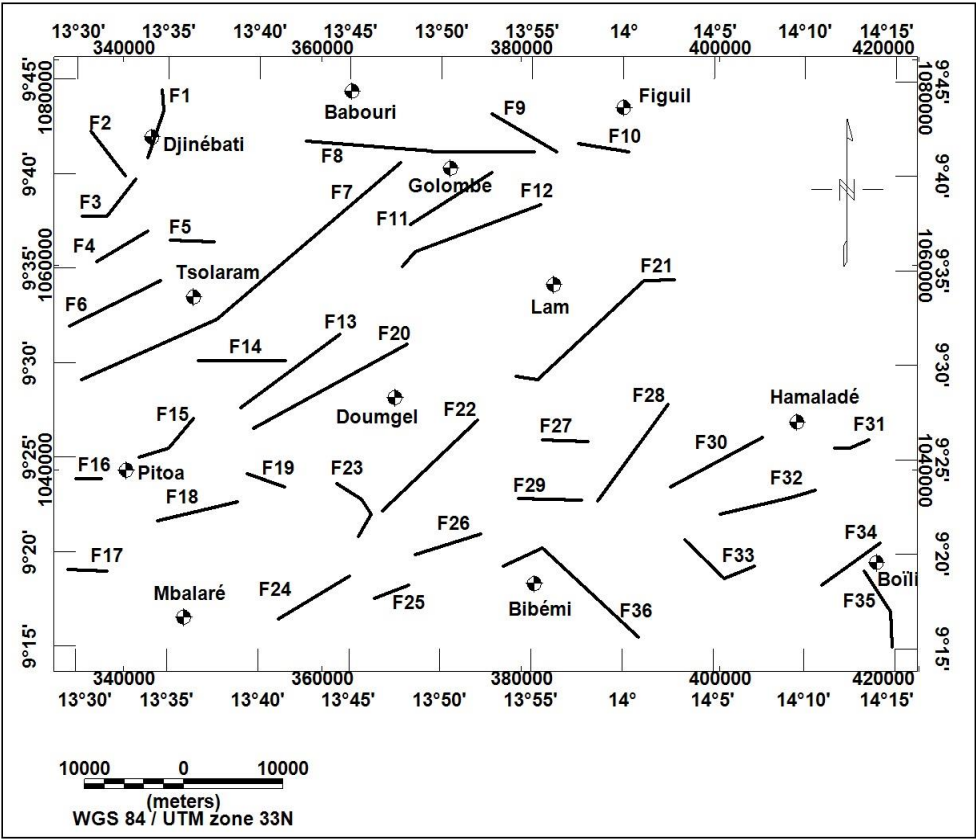242 formations.

243

244   **Figure 6: Euler's solutions map.**

245

246   Referring to the Blakely and Simpson (1986) method, the combined analysis of the Euler's
247 solution map (Fig. 6) and the superposition of peaks map (Fig. 5) obtained from the HGM and AS
248 maps permits us to generate the deep faults map (Fig. 7).
249   The faults map counts a total of 36 faults mainly directed to NW-SE, E-W and NE-SW. The Table 1
250   below presents the characteristics of some of these faults, namely their respective dip and depth.

251

252

253

254

Figure 7: Faults map resulting from Euler's solutions and HGM-AS maxima maps.

Dips are mainly N-W and the deepest faults are in the south of the surveyed area. The contact zone between biotite anatexite and migmatite gneisses formations is well marked by a large number of faults (F9, F12, F13, F15, F16 and F20).

Given its direction, the fault F7 could be associated to the tectonic line observed in western Golombe as it is shown in the geological map (Fig. 1).

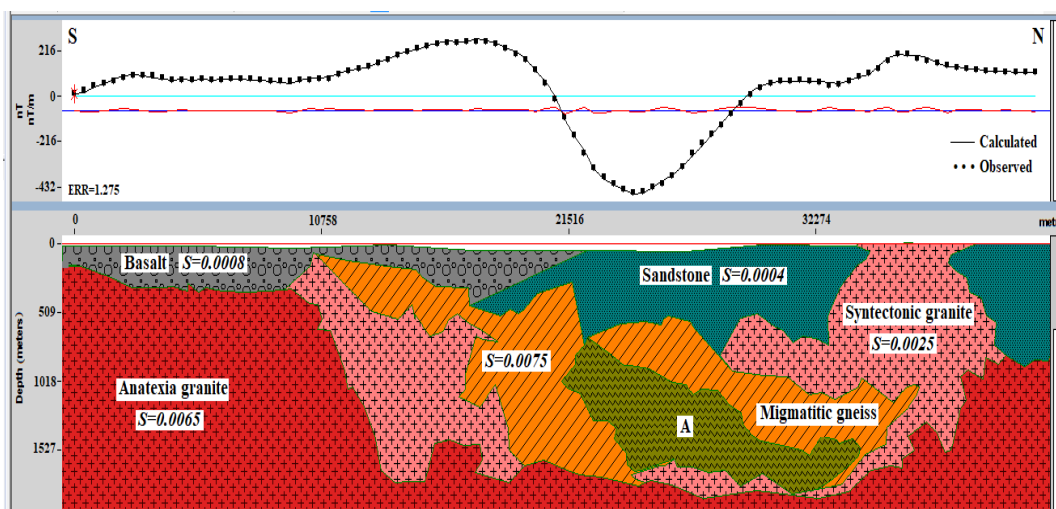| Faults	Dip	Depth (m)
F1	S-E	2600
F4	N-W	1400
F5	N	2000
F6	Vertical	1400
F7	Vertical	2500
F12	N-W	1500
F13	N-W	1400
F15	N-W	1900
F19	S	3000
F21	N-W	4300
F22	N-W	2600
F23	S-W	3500
F24	N-W	3300
F26	N-W	2500
F27	N	1800
F28	N-W	4700
F29	N	1400
F30	N-W	4500

271 **Table 1: Faults characterization of the studied area.**

272 **4.5. 2.75D magnetic models**

273   The two magnetic models (Fig. 8 and Fig. 9) are carried out respectively from profiles P1 and P2

274 drawn on the RTE map (Fig. 2). The earth's magnetic field, the declination, and the inclination of the

275 region were used as main input parameters. Referring to the geological map, the profile P1 over

276 cross from south to north: upper gneisses, monchiquite basalts of the Benue valley, rhyolitic tuffs,

277 alluviums, Kontcha sandstone conglomerate and anatexia granites. While the profile P2 extends

278 along the axis Djinébati-Mbalaré, over cross from the south to north: alluviums, migmatite gneisses,

279 biotite anatexite and anatexia granites. Magnetic properties for a given model layer, are assumed
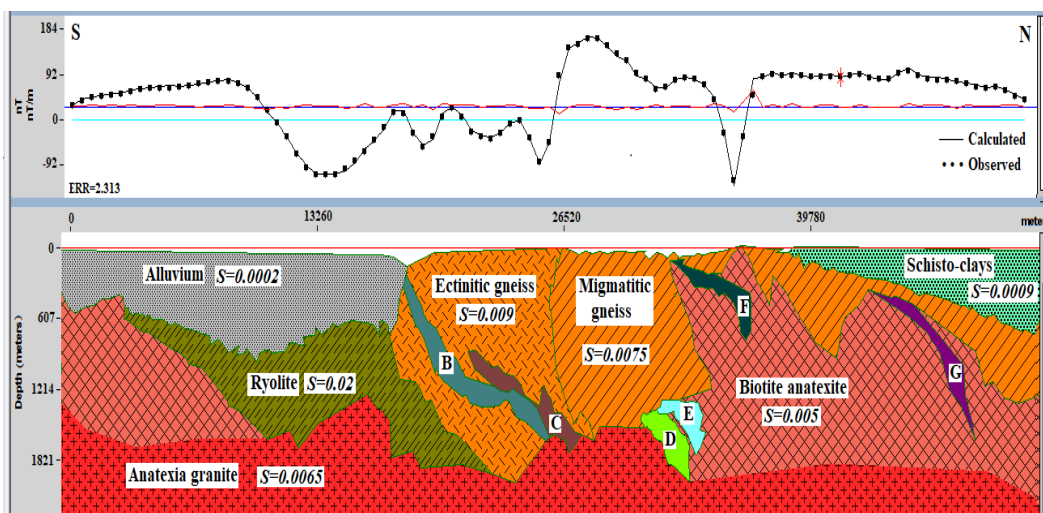
280 continuous and constant.

281

282
283 **Figure 8: 2.75D model obtained from profile P1.**

284
285

286
287 **Figure 9: 2.75D model obtained from profile P2.**

288

289 **4.5.1. Profile P1**

290   The profile P1 is 41370.7 metres long (X). According to Skalbeck et al. (2005), the strike lengths
291 is Y=31028.1 metres. Starting from south to north, the curve of the profile P1 passes through three
292 major anomalies on the RTE map: the first one (positive intensity) is at the northern Bibémi, the
293 second (negative) is in the Lam area and the third one (positive) is in the Figuil area. This justifies
294 the fact that this curve is in the form of a potential well (U-shape).

295   Regarding the layout of formations, we have a granitic basement whereas on the surface, basalt
296   rocks are distinctly separated from a sediments deposit, which correlates in part with the
297   information given by the geological map (Fig. 1) since this does not reveal the presence of basalt in
298   the northern Bibémi but rather in the Lam area. Given the lithology of the magnetic model, we can
299   also see that the syntectonic granite formation was set up well before the migmatite gneiss
300   formation. The previous formation is intruded by a large body A with a susceptibility value of S =
301   0.03 SI. Given its susceptibility (Clark and Emerson, 1991) and the environment in which it is found,
302   the body A could be diorite because gneiss with diorite composition is listed on the geological map
303   all around the studied area.

304   **4.5.2. Profile P2**

305   The profile P2 is 51867.4 metres long (X). According to Skalbeck et al. (2005), the strike lengths
306   is Y=38900.6 metres. Starting from south to north, the curve of the profile P2 passes through
307   several anomalies with variable wavelength from one to another alternatively positive and negative,
308   hence a much wavy curve with several peaks. This reflects the fact that this part of the studied area
309   has much more rugged subsurface. In other words, it has undergone many tectonic events, which
310   could be at the origin of several infiltrations from where the plurality of intrusive bodies observed in
311   layers.

312   The basement is made of granitic formation on which rests a biotite anatexite layer intruded by
313   three bodies E, F and G with respective susceptibility value of -0.0001, 0.015 and 0.007 SI. At this
314   layer, a formation of rhyolite is juxtaposed. On the surface we have an alluvial deposit which is
315   separated from the schisto-clays by two gneiss formations, namely ectinite gneiss and migmatite
316   gneiss. Ectinite gneiss is intruded by two bodies B and C with respective susceptibility value of -
317   0.003 and -0.00001 SI.

318   From these magnetic models, we deduce that our studied area rests on a granitic basement
319   which, according to the geological map, dates from the Precambrian period. The predominant rock
320   is migmatite gneisses which is a formation directly connected to the basement in some places.

321   Given the environment of intrusive bodies and their susceptibility value (Clark and Emerson,
322   1991), a suggestion on their nature is given in Table 2.

323

Rock	Susceptibility	Nature
A	0.03	Diorite
B	-0.0003	Calcite
C	-0.00001	Quartz
D	0.013	Diopside
E	-0.0001	Graphite
F	0.15	Pyroxenite
G	0.007	Amphibolite

324   **Table 2: Nature suggestion of intrusive bodies.**

325   **5. Discussion**

326   The choice of the window used for Euler's solutions is described by Marson and Klingele (1993).
327   According to these authors, the wavelength of the observed anomalies and the grid cell define the

Solid Earth
Discussions
Open Access
EGU

328   appropriate window size. Concerning the structural index (SI or N), Reid et al. (1990) concluded that
329   low values (0 and 1) provide the best estimations of depths for sills and dykes. In this case, we
330   focused on detection of anomaly sources, the determination of their depths and the localization of
331   faults and contacts in the studied area, that is why we have chosen a value of N = 1. Regarding
332   tolerance, we have set it at 15% because it is at this value that we observe a strong concordance
333   between Euler's solutions and their depths with many short and long length wave anomalies.
334   Concerning the Euler's solutions window, given the extent of structures in the region, we have
335   adopted a window size of "15 kmx15 km". As we are interested by deeper structures, the last three
336   methods above (HGM, AS and Euler Deconvolution) were applied to the upward continued RTE map
337   to remove the outcome of superficial bodies.

338   From all the magnetic techniques we have applied, it transpires that dykes and faulted folds
339   abound in the studied area. They are buried under diverse geological formations. Magnetic models
340   show that these formations, notably gneiss and anatexite biotite, are marked by numerous
341   intrusions.

342   The most of faults detected in the studied area were probably set up by the same event which
343   affected considerably the area. This event was certainly the reactivated Pan-African shear zones.

344   According to Njanko et al. (2010), the NE and NW structures in the studied area result from two
345   deformation processes recorded in the Pan-African belt, namely: senestral shearing and dextral
346   shearing. In addition, the N-S Gode-Gormaya shear zone (GGSZ) is probably also at the origin of
347   some highlighted faults (Ngako et al., 2008).

348   Faults with NE-SW dip are the most abundant. They are found in the area underlained by
349   migmatite gneisses and biotite anatexite formations. This is in accordance with the investigations of
350   Njandjock et al. (2006) for whom, most of faults in the studied area and surrounding areas are
351   covered by gneiss, sand or basalt. Magnetic models indicate the presence of basalts and gneisses on
352   the surface (Fig. 8 and 9), they are approving the thoughts of the authors above.

353   Furthermore, because of the same trending, the magnetic anomalies observed in the studied
354   area could also be the consequences of the Eburnean orogeny would have intensively modified the
355   northern Cameroon substratum. At the Cretaceous times, the setup of the Atlantic Ocean is one of
356   the most important events that affected the geodynamic evolution of the studied area (Nguimbous
357   et al., 2010). This event can also explain the opening of the above-mentioned faults and the very
358   upheaval layout of formations (vertical contacts) presented by magnetic models.

359

6. Conclusion

361   The purpose of this work was to help make the knowledge about Pitoa-Figuil basement easy
362   to understand. The combination of graphical methods (RTP) and analytical methods (HGM, AS, Euler
363   deconvolution) highlighted contact zones of some geological formations and permitted to locate
364   magnetic sources and estimate their depths related to shearing deformations. Results of these
365   complementary methods helped to characterize 18 faults in the studied area. Their major dip is N-
366   W. The location of boundary between the migmatite gneisses and biotite anatexite formations
367   given by the geological map is confirmed. After justifying the depth values of faults described by the
368   Euler deconvolution, magnetic models have shown that our studied area has undergone numerous

369 tectonic events (several intrusions). Most of the contacts are vertical. These models have also
370 taught us that the basement of our studied area is granitic, above which rest certain formations that
371 are flush with the surface. Furthermore, this study allowed us to suspect that, the settlement of the
372 Benue tectonic trough after the opening of the Atlantic, impacted the studied area subsurface in the
373 Northern Cameroon.

374 **Data Availability**
375 The data used to support the findings of this study are available from the corresponding author upon
376 request.

377 **Author Contribution**
378 Voltaire Souga Kassia performed the data analyses, modelling and preliminary interpretation including
379 preparation of the manuscript in conjunction with all the co-authors; Theophile Ndougsa-Mbarga
380 design the topic, gives the orientations for the investigation and reviewed the quality of the models and
381 related interpretation and the entire manuscript **;** Arsène Meying defines the criteria and the physical
382 parameters for the 2D3/4 modelling with the first author; Jean Daniel Ngoh and Steve Ngoa Embeng
383 have worked on the review of quality and quantitative analyses of respectively maps and 2D3/4 models.

384 **Competing Interest**
385 The authors declare that there are no conflicts of interest regarding the publication of this paper.

389 **References**
390 Awoyemi, M. O., Babatunde, A. A., Sesan, C. F., Abiodun, A. E., Sakiru, O. H., Olatunbosun, A. A., and
391 　　Chinwike, O. G.: Investigation of basement fault propagation in Chad Basin of Nigeria using
392 　　high resolution aeromagnetic data, International Journal of Geosciences, 7, 736-744, 2016.
393 Blakely, R. J. and Simpson, R. W.: Approximating Edges of Source Bodies from Magnetic or Gravity
394 　　Anomalies, Geophysics, 51, 1494-1498, 1986.
395 Clark, D. A. and Emerson, D. W.: Notes on rock magnetization characteristics in applied geophysical
396 　　studies, Exploration Geophysics, 22, 547–555, 1991.
397 Cordell, L. and Grauch, V. J.: Mapping basement magnetization zones from aeromagnetic data in the
398 　　San Juan Basin, New Mexico, 52nd Annual International Meeting, Society of Exploration
399 　　Geophysicists, Dallas, 246–248, 1982.
400 Daouda, D.: Les plutons de Guider et de Bossoum-Pologozom (chaîne panafricaine au Nord-
401 　　Cameroun) : analyses pétrographique, structurale, magnétique, géochronologique et
402 　　implications géodynamiques, Ph.D. thesis, Université de Toulouse, France, 261 pp., 2014.
403 Durrheim, R. J. and Cooper, R. J.: EULDEP: A Program for the Euler Deconvolution of Magnetic and
404 　　Gravity Data, Computers and Geosciences, 24, 6, 545-550, 1998.
405 Feumoe, A. N., Ndougsa Mbarga, T., Manguelle Dicoum, E., and Fairhead, D.: Delineation of
406 　　Tectonic Lineaments Using Aeromagnetic Data for the South-East Cameroon Area, Geofizika,
407 　　29, 175-192, 2012.

Solid Earth
Discussions

408   Jeng, Y., Lee, Y. L., Chen, C. Y., and Lin, J. M.: Integrated signal enhancements in magnetic
409   investigation in archaeology, Journal of Applied Geophysics, 53, 31–48, 2003.
410   Kamguia, J., Manguelle-Dicoum, E., Tabod, C. T., and Tadjou, J. M.: Geological models deduced from
411   gravity data in the Garoua basin, Cameroon, Journal of Geophysics and Engineering, 2, 2, 147-
412   152, 2005.
413   Khattach, D., Mraoui, H., Sbibih, D., and Chennouf, T. : Analyse multi-échelle par ondelettes des
414   contacts géologiques : application à la gravimétrie du Maroc nord oriental, Geosciences, 338,
415   521–526, 2006.
416   Keating, P. and Pilkington, M.: Euler deconvolution of the analytic signal and its application to
417   magnetic interpretation, Geophysical Prospecting, 52, 3, 165-182, 2004.
418   Leu, L. K.: Use of reduction to the equator process for magnetic data interpretation, Society of
419   Exploration Geophysicists, Los Angeles, Abstract P1.2, Geophysics, 47, 445, 1981.
420   Marson, I. and Klingele, E. E.: Advantages of using the vertical gradient of gravity for 3D
421   interpretation, Geophysics, 58, 1588-1595, 1993.
422   Ngako, V., Affaton, P., and Njongfang, E.: Pan-African Tectonics in Northwestern Cameroon,
423   Implication for the History of Western Gondwana, Gondwana Research, 14, 509-522, 2008.
424   Nguimbous Kouoh, J. J., Ndougsa Mbarga, T., Njandjock Nouck, P., Eyike, A., Campos-Enriquez, J. O.,
425   and Manguelle-Dicoum, E.: The structure of the Goulfey-Tourba sedimentary basin (Chad-
426   Cameroon): a gravity study, Geofisica Internacional, 49, 4, 412-425, 2010.
427   Njandjock Nouck, P., Manguelle-Dicoum, E., Ndougsa Mbarga, T., and Tabod, T. C.: Spectral analysis
428   and gravity modelling in the Yagoua, Cameroun, sedimentary basin, Geofisica Internacional,
429   45, 2, 209-215, 2006.
430   Njanko, T., Nédélec, A., Kwékam, M., Siqueira, R., and Esteban, L.: Emplacement and Deformation of
431   the Fomopéa Pluton: Implication for the Pan-African History of Western Cameroon, Journal of
432   Structural Geology, 32, 306-320, 2010.
433   Ntsama, A. J., Bessong, M., Hell, J. V., Mbesse, C. O., Nolla, J. D., Dissombo, A. N., Edimo, Eyong, J. T.,
434   Mbassa, B. J., Mouloud, B. I., Vignaud, P. J., and Mfoumbeng, M. P.: The Importance of
435   Diagenetic Processes in Sandstones Facies of the Hamakoussou Sedimentary Basin in North
436   Cameroon: Influence on Reservoir Quality, International Journal of Sciences, Basic and Applied
437   Research, 13, 2, 220-230, 2014.
438   Paterson, Grant, and Watson Ltd.: Études aéromagnétiques sur certaines régions de la République
439   Unie du Cameroun. Rapport d'interprétation : Agence Canadienne de Développement
440   International, Toronto, Canada, 1976.
441   Phillips, J. D.: Processing and Interpretation of Aeromagnetic Data for the Santa Cruz Basin-
442   Patagonia Mountain Area, South Central Arizona, US Geological Survey, Open File Report, 02-
443   98, 2001.
444   Rasmussen, R. and Pedersen, L. B.: End corrections in potential field modelling, Geophysical
445   Prospecting, 27, 749–760, 1979.
446   Roest, W. R., Verhoef, J., and Pilkington, M.: Magnetic interpretation using the 3D analytic signal,
447   Geophysics, 57, 116–125, 1992.

448   Skalbeck, J. D., Karlin, R. E., Shevenell, L., and Widmer, M. C.: Gravity and aeromagnetic modelling
449   of alluvial basins in the southern Truckee Meadows adjacent to the Steamboat Hills
450   geothermal area, Washoe County, Nevada, Geophysics, 70, 3, 81-89, 2005.

451   Talwani, M. and Heirtzler, J. R.: Computation of magnetic anomalies caused by two-dimensional
452   bodies of arbitrary shape, In: Parks G. A. (ed.)-Computers in the Mineral Industries, Part 1,
453   Stanford University Publications, Geological Sciences, 9, 464–480, 1964.

454   Toteu, S. F., Penaye, J., and Poudjom, Y. D.: Geodynamic Evolution of the Pan-African Belt in Central
455   Africa with Special Reference to Cameroon, Canadian Journal of Earth Sciences, 41, 73-85,
456   2004.

457   Whitehead, N. and Musselman, C.: Processing, Analysis and Visualization System for 3D Inversion of
458   Potential Field Data in Oasis montaj v6.1. Montaj Grav/Mag Interpretation,
459   https://fr.scribd.com/document/349623750/montajGravMagInterpretation-pdf/, last access:
460   11 June 2020, 2005.